Ultrasound in Medicine & Biology 49 (2023) 1550–1560

Contents lists available at ScienceDirect

Ultrasound in Medicine & Biology

journal homepage: www.elsevier.com/locate/ultrasmedbio

Original Contribution

Ambient Pressure Sensitivity of the Subharmonic Response of Coated Microbubbles: Effects of Acoustic Excitation Parameters

Roozbeh H. Azami [a], Flemming Forsberg [b], John R. Eisenbrey [b], Kausik Sarkar [a,*]

[a] Department of Mechanical and Aerospace Engineering, George Washington University, Washington, DC, USA
[b] Department of Radiology, Thomas Jefferson University, Philadelphia, PA, USA

ARTICLE INFO

Keywords:
Ambient pressure sensitivity
Subharmonic-aided pressure estimation
Ultrasound contrast agents
Lipid-coated microbubbles

Objective: The sensitivity of the acoustic response of microbubbles, specifically a strong correlation between their subharmonic response and the ambient pressure, has motivated development of a non-invasive subharmonic-aided pressure estimation (SHAPE) method. However, this correlation has previously been found to vary depending on the microbubble type, the acoustic excitation and the hydrostatic pressure range. In this study, the ambient pressure sensitivity of microbubble response was investigated.
Methods: The fundamental, subharmonic, second harmonic and ultraharmonic responses from an in-house lipid-coated microbubble were measured for excitations with peak negative pressures (PNPs) of 50–700 kPa and frequencies of 2, 3 and 4 MHz in the ambient overpressure range 0–25 kPa (0–187 mmHg) in an *in vitro* setup.
Results: The subharmonic response typically has three stages—occurrence, growth and saturation—with increasing excitation PNP. We find distinct decreasing and increasing variations of the subharmonic signal with overpressure that are closely related to the threshold of subharmonic generation in a lipid-shelled microbubble. Above the excitation threshold, that is, in the growth-saturation phase, subharmonic signals decreased linearly with slopes as high as −0.56 dB/kPa with ambient pressure increase; below the threshold excitation (at atmospheric pressure), increasing overpressure triggers subharmonic generation, indicating a lowering of subharmonic threshold, and therefore leads to an increase in subharmonic with overpressure, the maximum enhancement being ~11 dB for 15 kPa overpressure at 2 MHz and 100 kPa PNP.
Conclusion: This study indicates the possible development of novel and improved SHAPE methodologies.

Introduction

Microbubbles in the diameter range 1–10 μm are used as contrast-enhancing agents for imaging as well as for drug delivery purposes [1,2]. Depending on the excitation amplitudes, the microbubbles can generate harmonic, ultraharmonic and subharmonic responses in addition to the fundamental response relative to the excitation [3,4]. These signals have led to the development of novel imaging modalities with potentially high signal-to-noise ratios [1]. Subharmonic imaging (SHI) using the subharmonic frequency band has been a promising candidate in this endeavor [5–12]. Additionally, the subharmonic amplitude is influenced by surrounding fluid pressure, which may enable non-invasive measurement of the local blood pressure in critical organs [13–15]. Here, we study the subharmonic response from a lipid-coated microbubble as a function of overpressure for different excitation amplitudes and frequencies.

Early proposals to use microbubbles as a minimally invasive pressure sensor studied hydrostatic pressure-dependent variations in the resonance frequency [16–18], a single bubble's echo [19] and disappearance time of gas bubbles [20]. However, the lack of sensitivity and accuracy hindered the further development of these methods for clinical applications. Shi et al. [21] first reported the high sensitivity of the subharmonic response of Levovist microbubbles to hydrostatic pressures in the physiological range (0–186 mmHg), leading them to propose subharmonic-aided pressure estimation (SHAPE). SHAPE has been investigated in animal and human trials with promising results in measuring left ventricular pressure [22], interstitial fluid pressure in tumors [23,24] and portal hypertension in animals and humans [25–27].

In contrast to harmonics, which rise continuously with increasing excitation, subharmonic responses are only generated above a frequency-dependent excitation threshold [28]. Shi et al. [21] reported three stages of subharmonic production—occurrence, growth and saturation—with the maximum reduction in subharmonic signals under 200 mmHg overpressure occurring in the rapid growth stage. Subsequently, the sensitivity of the subharmonic to ambient pressure has been the subject of numerous research studies. Table 1 summarizes important findings of *in vitro* experiments focusing on acoustic excitation parameters and the range of overpressures.

Table 1 indicates that the subharmonic amplitude was observed to decrease with ambient pressure for almost all conditions and bubbles.

* Corresponding author. Department of Mechanical and Aerospace Engineering, George Washington University, 800 22nd Street NW, Suite 3000, Washington, DC 20052, USA.
E-mail address: sarkar@gwu.edu (K. Sarkar).

https://doi.org/10.1016/j.ultrasmedbio.2023.02.019
Received 11 November 2022; Revised 20 January 2023; Accepted 27 February 2023

Table 1
Summary of *in vitro* studies on the ambient pressure sensitivity of subharmonic signal

Study	Agent (shell/core)	Over-pressure (kPa)	Excitation frequency (MHz)	PNP (kPa)	Trend	Maximum change/sensitivity
Kalayeh et al. [55]	Experimental (lipid/C_3F_8)	2–9.8	5	178	Decrease	0.56 dB/kPa
Qiao et al. [51]	SonoVue (lipid/SF_6)	2.6–21.3	5	238–454	Decrease	1.84 dB/kPa
Xu et al. [30]	SonoVue	1–5	4	20–300	Increase	1.23 dB/kPa
				400–520	Decrease	1.15 dB/kPa
Nio et al. [31]	SonoVue	0–10	1.7–7	25–300	Increase	1.23 dB/kPa
		16–26			Decrease	1.23 dB/kPa
Li et al. [47]	SonoVue	1–24	4	350–500	Decrease	0.84 dB/kPa
			1.33	350		0.75 dB/kPa
Frinking et al. [29]	Experimental (lipid/C_4F_{10})	0 and 24	4	20–350	Increase	28.4 dB
				350–800	Decrease	9.6 dB
		0–16		50	Increase	~25 dB
Faez et al. [33]	BR14 (lipid/C_4F_{10})	−15 to +15	5	156	Both	+10 dB
			10	240		
Sun et al. [56]	SonoVue	0–25	4	300	Decrease	0.54 dB/kPa
			1.33		Increase	14.1 dB
Halldorsdottir et al. [57]	Sonazoid (lipid/C_4F_{10})	0–25	2.5–6.6	175–300[a]	Decrease	14.9 dB
	Definity (lipid/C_3F_8)					13.3 dB
	Optison (albumin/C_3F_8)					11.2 dB
	Levovist (galactose/air)		4.4	210[a]		~10 dB
	ZFX (Lipid/C_4F_{10})					12 dB
Shi et al. [21]	Levovist	0–25	2	390	Decrease	9.6 dB
		0 and 13		320–540		~ 5 dB
		0 and 27				11.3 dB
Halldorsdottir et al. [23]	Definity	0–6.6	10	120–751[a]	Decrease	11.4 dB (1.69 dB/kPa)
			6.7	165–840[a]		10.23 dB
Andersen and Jensen [58]	SonoVue	0–25	4	485	Decrease	0.42 dB/kPa[b]
				500		0.42 dB/kPa[b]
Adam et al. [59]	Optison	0–20	4	200	Decrease	0.54 dB/kPa
Dave et al. [60]	Sonazoid	0–16	2.5	76–897	Decrease	8.1 dB

PNP, peak negative pressure.
[a] Acoustic pressures converted from the reported peak-to-peak values.
[b] The ratio of subharmonic energy to fundamental energy was investigated.

However, a few cases also exhibit an increase with overpressures primarily at low excitations. Frinking et al. [29] first reported an increase in subharmonic signal at low-amplitude acoustic excitations when the ambient overpressure was changed from 3 to 180 mmHg. They attribute it to an enhanced compression-only behavior caused by ambient overpressure. Both decrease and increase in subharmonic amplitudes with overpressure were observed for SonoVue microbubbles [30,31], claimed to be caused by a reduction in surface tension, microbubble destruction under elevated overpressures and the SF6 gas core [31,32]. Faez et al. [33] used a 2.5 kHz acoustic wave to dynamically manipulate the ambient pressure with a peak of 15 kPa and found that the subharmonic response of microbubbles can either increase or decrease with ambient pressure. Using the Marmottant model [34], they related the behaviors to the shell material properties, including initial surface tension. The shell properties have been shown to change with overpressure [35–37].

Intuitively, one would expect an ambient pressure increase to restrict bubble activities, leading to a reduction of its subharmonic response. However, ambient pressure also changes the natural frequency of the bubble as well as the characteristic frequency of maximum subharmonic response (typically twice the resonant frequency, but it differs for coated microbubbles because of enhanced damping [38,39]). Therefore, depending on the excitation frequency, increasing overpressure could result in oscillations approaching (or moving away from) subharmonic resonance, resulting in increasing (or decreasing) subharmonic response, as we previously determined using Rayleigh–Plesset dynamics [40]. There we found that for a free bubble, subharmonic signals decreased with increasing overpressure for the excitation frequency normalized by the natural frequency being in the range of 1.4–1.6, but increased for the frequency ratio >2.1; it was non-monotonic in the intermediate range. Consequently, the varying trends in past experiments, which were often limited in their range of overpressure and excitation parameters, warrant further investigation.

Our aim here was to explore the ambient pressure sensitivity of microbubbles' acoustic response in a wide range of acoustic parameters (peak negative pressure [PNP] of 50–700 kPa and excitation frequencies of 2, 3 and 4 MHz) covering all three stages of subharmonics and at ambient overpressure (0-25 kPa) corresponding to the physiological blood pressure range (0–186 mmHg). We also studied the fundamental, second harmonic and ultraharmonic (3/2 order) varying overpressure and acoustic parameters.

Methods

Microbubbles

Lipid-shelled microbubbles with a perfluorobutane (C_4F_{10}) gas core were synthesized according to a protocol described in our previous study [41]. 1,2-Dipalmitoyl-*sn*-glycero-3-phosphatidylcholine (DPPC) and 1,2-dipalmitoyl-*sn*-glycero-3-phosphatidylethanolamine–polyethyleneglycol-2000 (DPPE-PEG-2000, Avanti Polar Lipids, Alabaster, AL, USA) were used to create microbubbles with a shell composition of 90% DPPC –10% DPPE-PEG2000 molar ratio and C_4F_{10} (FluoroMed L.P., Round

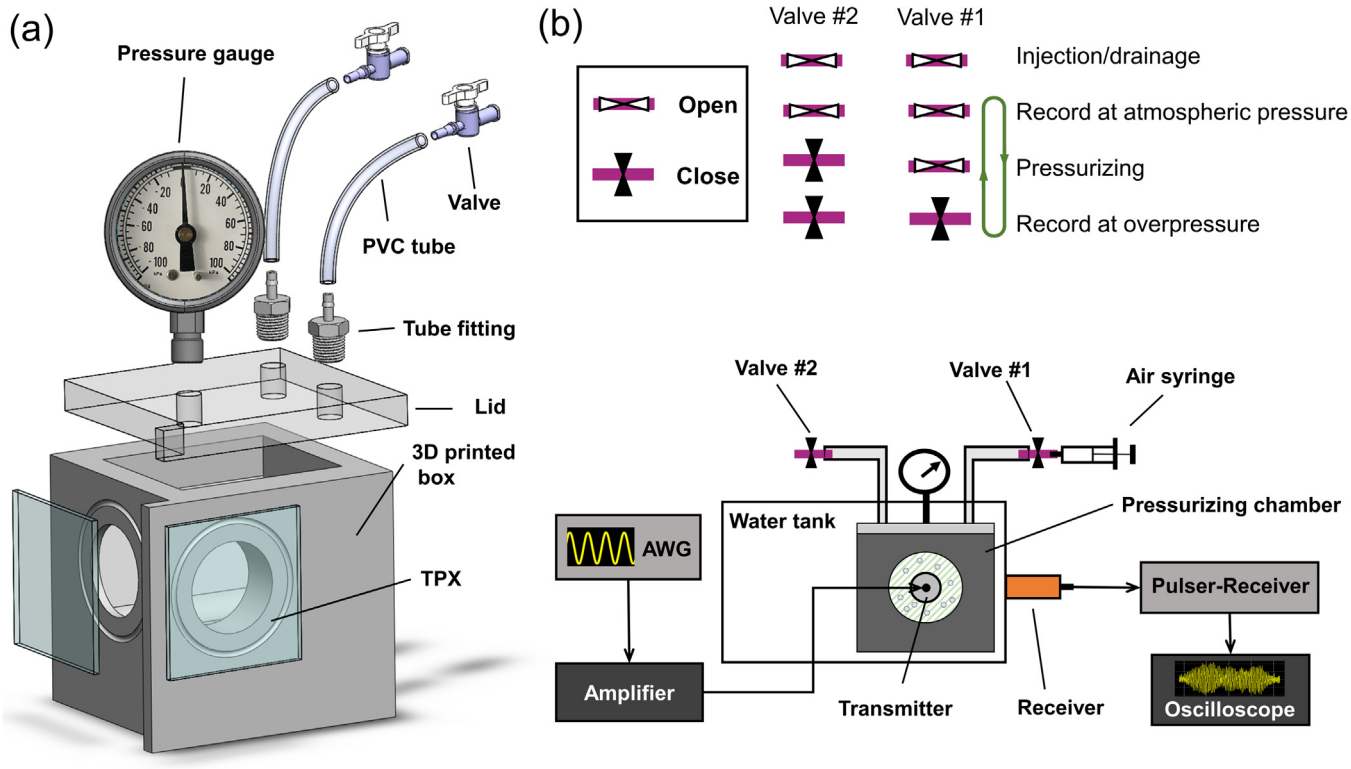

Figure 1. (a) Exploded view of the pressurizing chamber. (b) Instrumentation and pressurizing sequence used for microbubble response measurement at different ambient overpressures. AWG, arbitrary wave generator; PVC, polyvinyl chloride.

Rock, TX, USA) core. The mechanical agitation method was used to produce microbubbles. We had previously measured the size distribution of this microbubble (with 10% PEG), finding a 2.2 μm mean diameter with 99% of microbubbles less than 10 μm in diameter [41]. It can be referred to for the details of the size distribution.

Experimental setup

Figure 1 illustrates the experimental setup used for this study. Microbubble signals at different hydrostatic pressures were measured using a pressurizing chamber sustaining overpressures of 0–25 kPa. A rectangular open box (40 W × 40 H × 45.2 D mm) was 3-D printed from micro-carbon fiber-filled nylon composite (Onyx, Markforged, Watertown, MA, USA). Two circular extruded cut holes were incorporated into the side walls as acoustic windows. Rigid 2 mm thick plaques of polymethylpentene (PMP), commercially known as TPX (TPX RT18, Mitsui Chemicals America Inc., Rye Brook, NY, USA), were glued using instant adhesive gel (Loctite 454, Henkel Corp., Stamford, CT, USA) to the exterior of the acoustic windows, ensuring proper sealing and adhesion. Bulging of the acoustic window plate under hydrostatic pressure and consequent interference in ultrasound were avoided because of the high flexural strength (47 MPa) of the TPX plaques. The TPX plaques (acoustic impedance = 1.79 MRayl) provided a good impedance match to water (acoustic impedance = 1.48 MRayl). The insertion loss of the TPX plaques is discussed in a later section. An acrylic lid (40 W × 7 H × 45.2 D mm) was glued to the 3-D-printed box to accommodate a pressure gauge (range: −100 to 100 kPa; Ashcroft, Stratford, CT, USA) and two stainless-steel fittings (Part No. 4406T16, McMaster-Carr, Elmhurst, IL, USA) were connected to polyvinyl chloride (PVC) tubes (Part No. 5233K52, McMaster-Carr) as injection/drainage and pressurizing ports. Stopcock on/off valves (Part No. 7033T25, McMaster-Carr) were attached to tubes opening to control the pressurizing sequence (Fig. 1b). An air-filled syringe was used to manually apply overpressure inside the chamber through a Luer lock connection to the valve. A magnetic stir bar was placed in the bottom of the pressurizing chamber to gently stir the microbubble solution during experiments.

The pressurizing chamber was placed in an acrylic water tank (120 W × 140 H × 120 D mm) with ultrasonic transducers embedded in the walls (Fig. 1b). 5 MHz (V309, Olympus, Waltham, MA, USA) and 2.25 MHz (V306, Olympus) single-element focused transducers with a 30.5 mm focal length and 12.7 mm element size were used to transmit acoustic waves of 2, 3 and 4 MHz frequencies. An arbitrary wave generator (AWG) (DG1022, RIGOL, Portland, OR, USA) was used to generate 32-cycle sine bursts of desired frequency and amplitude at a 100 Hz pulse repetition frequency (PRF). The AWG signal was amplified by a 55 dB power amplifier (A150, Electronics & Innovation, Rochester, NY, USA) and used to drive the transmitter. Echoes from microbubbles were received by a cylindrically focused hydrophone (Y-102, Sonic Concepts, Bothell, WA, USA) with 50 mm geometric focus, 17.5 mm active diameter and an operating frequency range of 10 kHz to 20 MHz. Foci of transmitting and receiving transducers coincided perpendicularly inside the pressurizing chamber. The received signal was conditioned by an ultrasonic pulser–receiver (Model 5800, Panametrics, Olympus) and acquired in sample mode by an oscilloscope (MDO 3024, Tektronix, Beaverton, OR, USA) connected to a desktop computer. A MATLAB (The MathWorks, Natick, MA, USA) program captured 20 voltage–time traces, and the power spectra obtained by the Fast Fourier transform were averaged.

Calibration of transducers

Focused transducers were calibrated at each frequency employed using a capsule hydrophone (HGL0200, Onda Corp., Sunnyvale, CA, USA) according to a similar procedure described previously [42]. The focused transducer and the capsule hydrophone were placed in a water tank (95 W × 82 H × 300 D mm) filled with de-gassed water. To include the effect of the acoustic window on the transmitted ultrasound, a TPX plaque 2 mm thick was placed normally at 10 mm in front of the transducer, ensuring an accurate pressure environment as in the experimental setup. The

Table 2
Insertion loss of 2-mm-thick TPX plaque measured at different frequencies

Excitation frequency (MHz)	Insertion loss (dB)
1	0.38 ± 0.18
1.5	0.50 ± 0.20
2	0.86 ± 0.23
2.5	1.17 ± 0.15
3	1.88 ± 0.29
3.5	1.75 ± 0.05
4	2.02 ± 0.14
4.5	1.95 ± 0.10
5	2.14 ± 0.13
5.5	2.48 ± 0.03
6	2.80 ± 0.14
6.5	2.76 ± 0.10
7	2.96 ± 0.13
7.5	3.25 ± 0.13
8	3.92 ± 0.22

hydrophone was placed in the focal zone of the transducer using a holder attached to a three-axis translation stage (Newport, Irvine, CA, USA). The focused transducer was driven using 32-cycle sine bursts generated and amplified by the AWG and the power amplifier. The hydrophone's signal was pre-amplified (AH-2010, Onda Corp.) before it was visualized by the oscilloscope and recorded for pressure calculations.

Insertion loss of TPX window

To compensate for the effect of the acoustic window on the received signals, the insertion loss (IL) of the TPX plaque was measured using a narrowband through-transmission substitution method [43,44]. A 5 MHz unfocused transducer (V309, Olympus) was used along with a sine burst of 50 mV peak-to-peak amplitude generated and amplified by the AWG and the power amplifier. Hydrophone signals were recorded with and without a TPX sheet placed 10 mm apart from the hydrophone tip. The insertion loss was calculated as [45]

$$\mathrm{IL} = 20\log(A_{wo}/A_w)$$

where A_{wo} and A_w are the amplitudes of the received signal spectra without and with TPX plaque, respectively. Insertion loss values measured for the frequency range 1–8 MHz are reported in Table 2 and were used to correct the microbubble response at relative frequencies.

Experimental procedure

To measure the effect of ambient overpressure on the response of microbubbles, 120 mL of diluted microbubble solution (~ 30,000 microbubbles/mL [41]) was transferred into the pressurizing chamber so that the acoustic windows were fully submerged, and a narrow air gap was left under the chamber ceiling (ports and pressure gauge socket). This air gap allowed convenient adjustment of the overpressure inside the chamber using a 20 mL air syringe. The value indicated by the pressure gauge was considered as the hydrostatic overpressure sensed by the microbubbles. The dilution factor used here (~160,000) exhibited a strong active signal compared with other dilutions tested before starting the study. Next, the pressurizing chamber was placed in the water tank in a way that acoustic windows were normal to the ultrasound path (Fig. 1b). A 1 cm thick plastic sheet with an impression of the bottom of the chamber etched was used to ensure the orientation and alignment of the pressurizing chamber with the transducers over all experiments.

The pressurizing sequence and corresponding valve conditions are illustrated in Figure 1b. First, the microbubbles' response to an acoustic excitation was recorded at atmospheric pressure with all valves open (0 kPa overpressure). In the next step, the pressure inside the chamber was increased by air syringe, and all valves were closed after the desired overpressure (either 5, 10, 15, 20 or 25 kPa) was reached. Once the microbubbles' response under hydrostatic overpressure was recorded, the pressure inside the chamber was released for the next recording. This sequence was repeated eight times for the same overpressure, recording the difference of their averages from the zero-overpressure value. Total experiment time for the eight repeats was approximately 3 min, and the bubble suspension was prepared about 30 s beforehand. The chamber was then drained, and the microbubble solution was refreshed. Measurements at each setting (overpressure, frequency, acoustic pressure) were replicated three times. An unpaired *t*-test was employed to determine whether the difference between acoustic

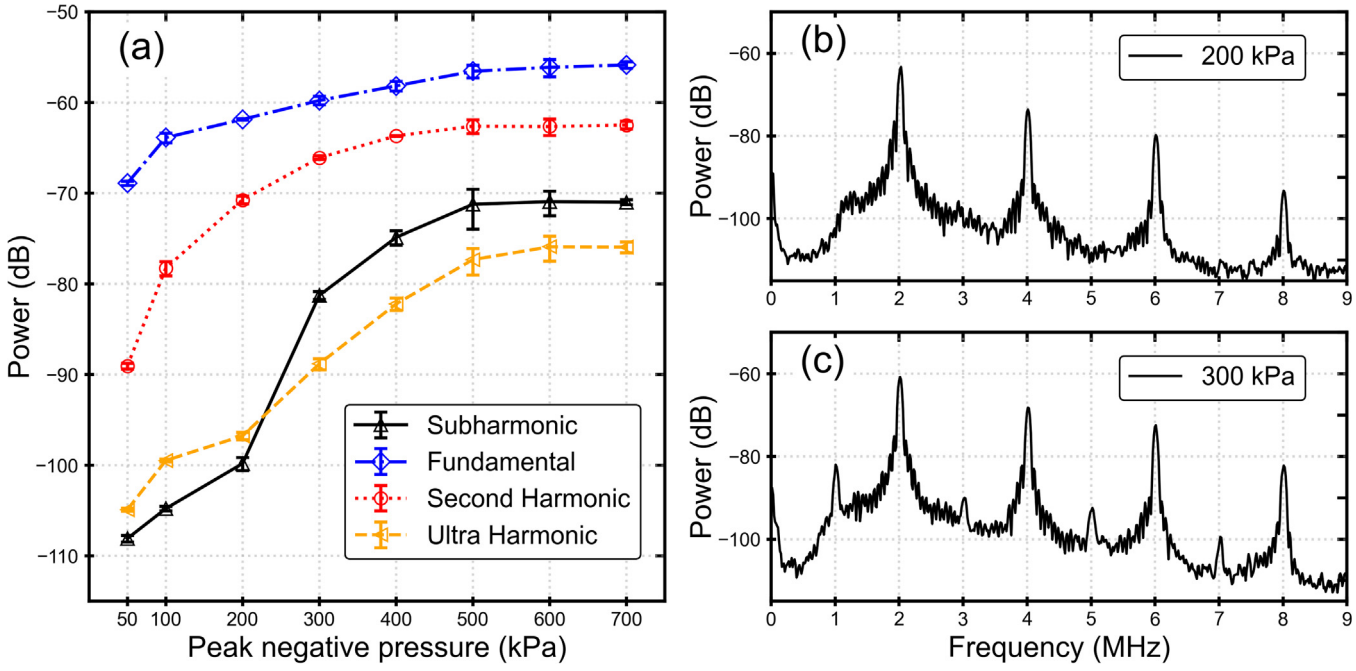

Figure 2. (a) Scattered response of microbubbles as a function of peak negative pressure at 2 MHz excitation and 0 kPa overpressure. (b, c) Example power spectra at acoustic pressures of (b) 200 kPa and (c) 300 kPa reveal the subharmonic thresholding behavior.

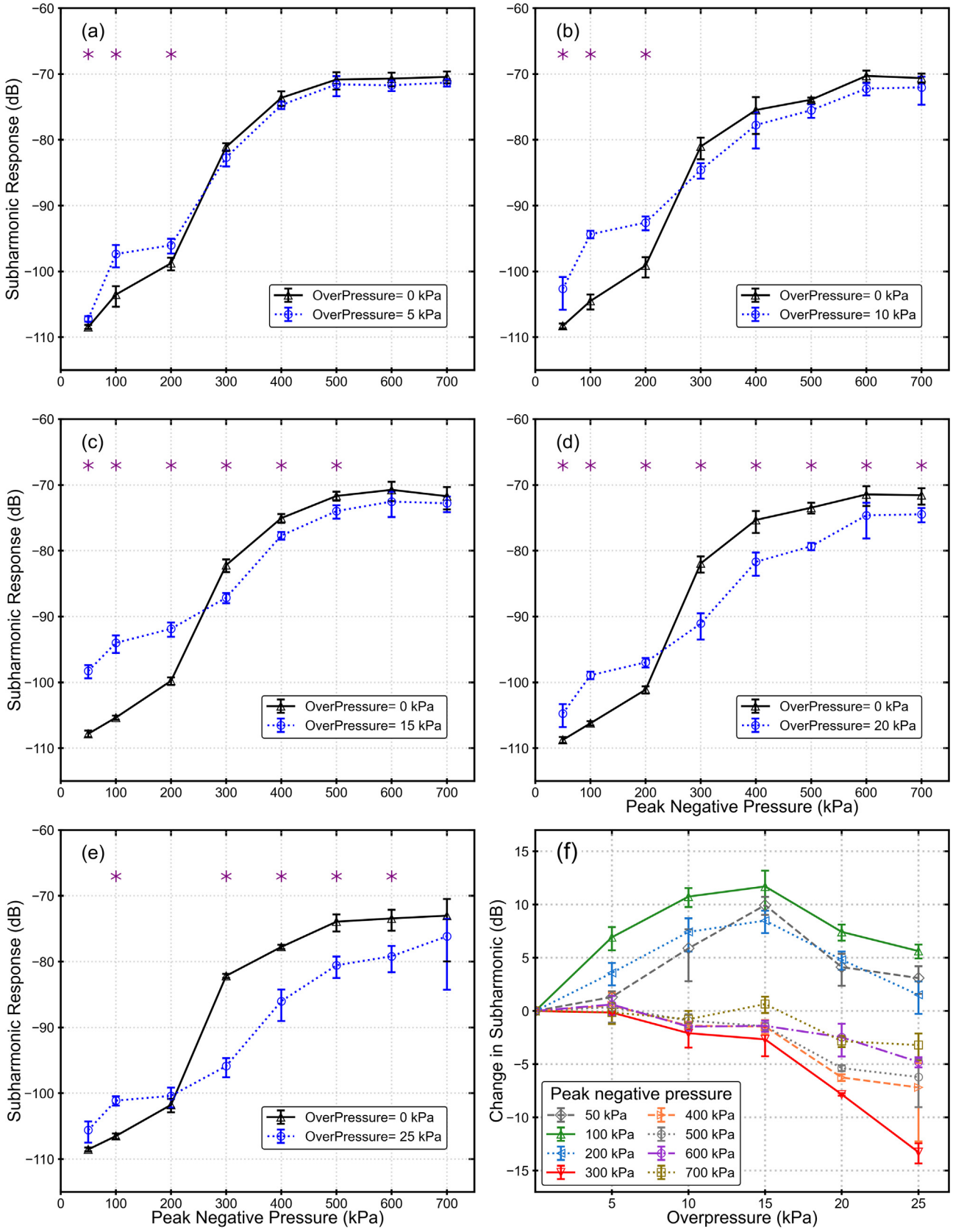

Figure 3. (a–e) Effect of overpressures of (a) 5 kPa, (b) 10 kPa, (c) 15 kPa, (d) 20 kPa and (e) 25 kPa on subharmonic response of microbubbles at 2 MHz excitation plotted against acoustic peak negative pressure. (f) Change in subharmonic amplitude plotted as a function of overpressure at 2 MHz excitation frequency revealing distinct different trends. Statistically significant difference ($p < 0.05$) between response at atmospheric pressure and overpressure is denoted by an asterisk at the corresponding peak negative pressure.

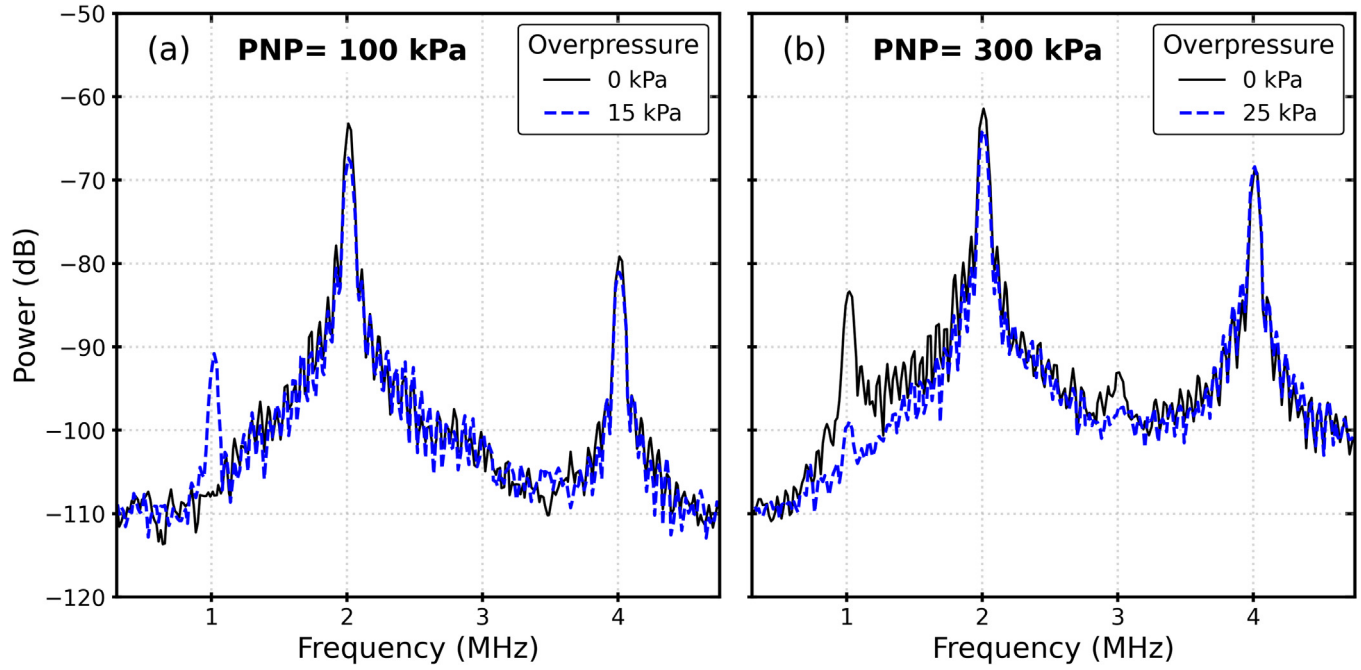

Figure 4. Frequency response of microbubbles before (*solid black line*) and after (*dashed blue line*) applying overpressure at 2 MHz frequency: (a) 100 kPa acoustic peak negative pressure (PNP) and 15 kPa overpressure; (b) 300 kPa acoustic PNP and 25 kPa overpressure.

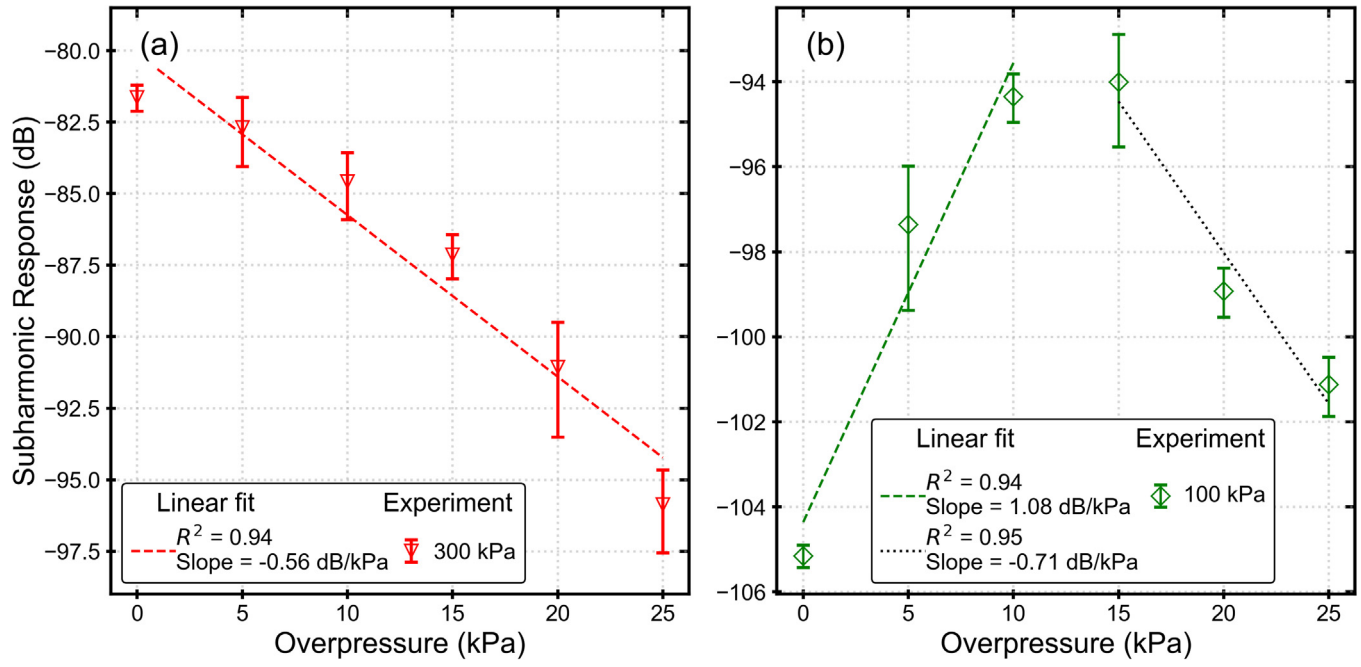

Figure 5. Linear fit to subharmonic data with strongest subharmonic ambient pressure sensitivities at 2MHz excitation frequency. (a) Linear decrease in subharmonic at 300 kPa acoustic pressure. (b) Non-monotonic increase in subharmonic at 100 kPa acoustic pressure.

responses at atmospheric pressure and overpressure is statistically significant ($p < 0.05$).

Results

Figure 2a illustrates the scattered power from the in-house microbubbles as a function of acoustic peak negative pressure at atmospheric pressure (0 kPa overpressure) and 2 MHz frequency excitation. Each data point is the corrected averaged peak value of the power spectrum using the acoustic window insertion loss values summarized in Table 2. The fundamental, which is the strongest, and the second harmonic responses increase gradually with the increase in peak negative pressure. However, the subharmonic and ultraharmonic responses exhibit a threshold behavior indicating occurrence, growth and saturation. Before occurrence (Fig. 2b), the subharmonic amplitude is close to the noise level. Then it experiences a significant jump, which marks the beginning of the growth stage beyond 200 kPa acoustic pressure (Fig. 2c). The thresholds for growth of subharmonic and ultraharmonic lie between 200 and 300 kPa peak negative pressures.

The effect of overpressure on the subharmonic response at 2 MHz frequency excitation is illustrated in Figure 3. For excitations corresponding to before occurrence (PNP $\leq$ 200 kPa), applying overpressure

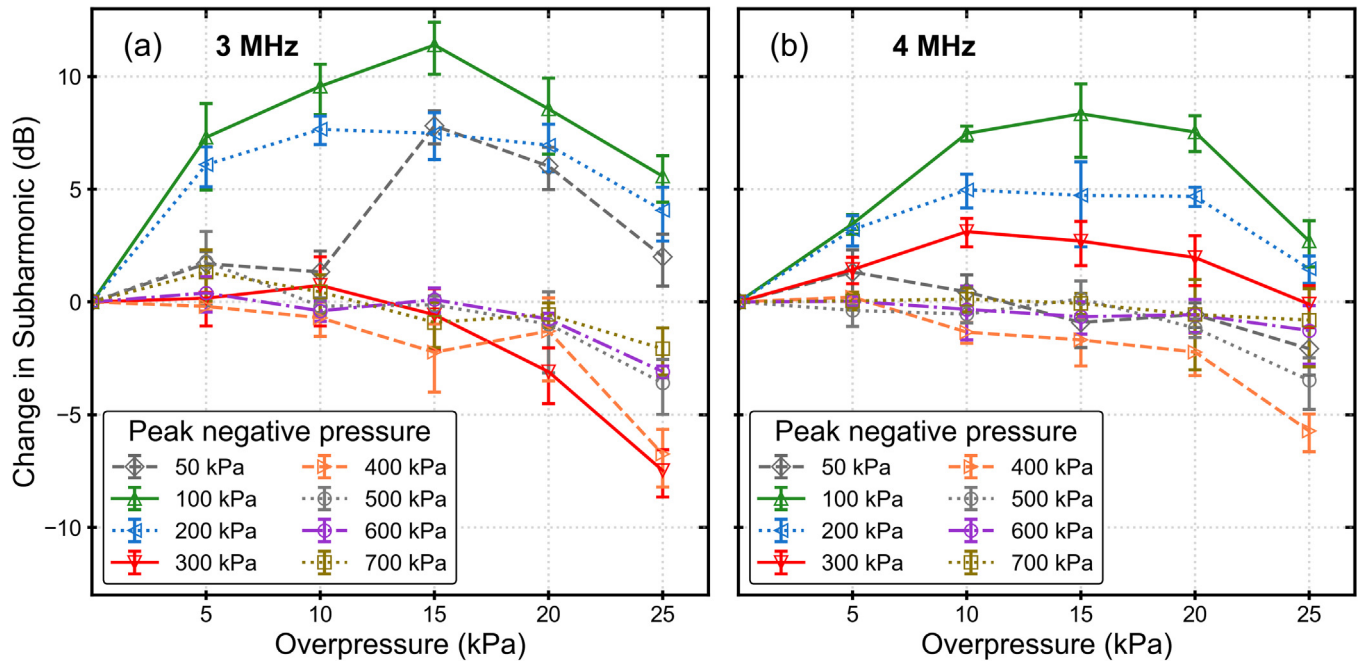

Figure 6. Change in subharmonic as a function of overpressure for 50 to 700 kPa peak negative pressures and (a) 3 MHz and (b) 4 MHz excitation frequencies.

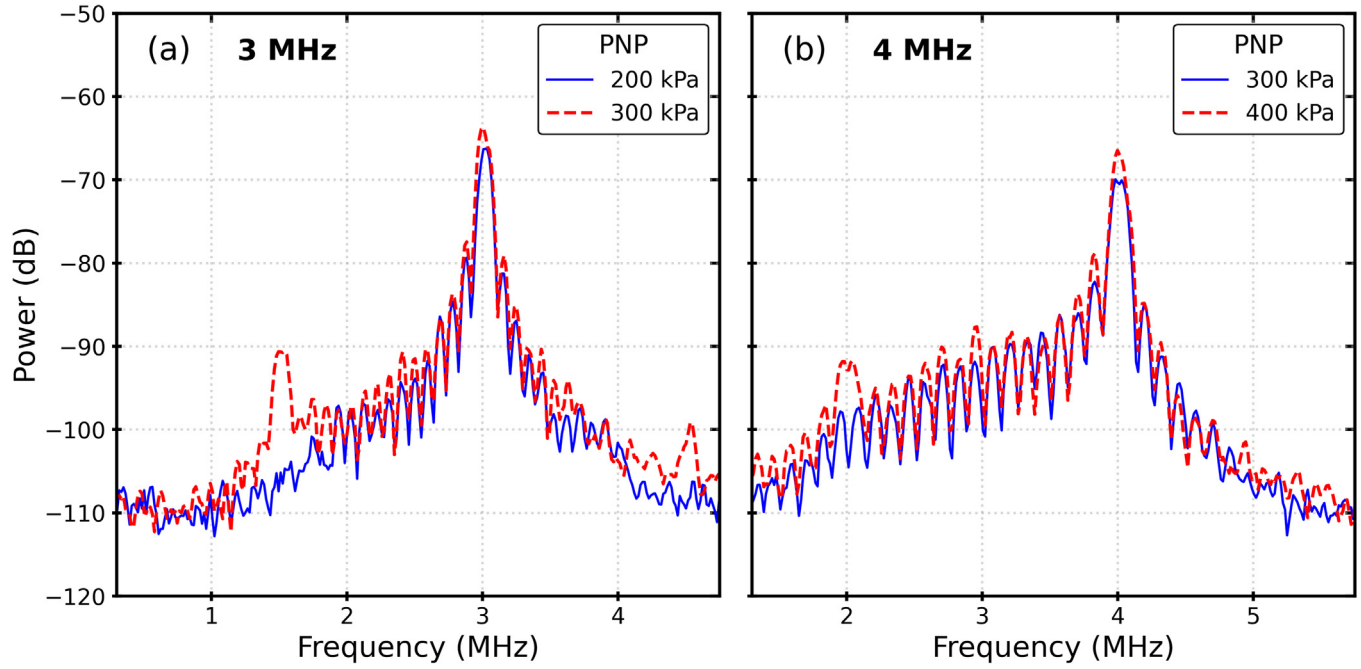

Figure 7. Frequency response at atmospheric pressure before and after subharmonic sensitivity transition point: (a) 3 MHz; (b) 4 MHz. PNP, peak negative pressure.

enhanced the subharmonic in comparison to the atmospheric condition (0 kPa overpressure). In contrast, for excitations in the growth and saturation stages (PNP >200 kPa), subharmonic amplitude decreased with overpressure. Figure 3f illustrates the features observed for all cases in which the enhancement of subharmonic (with increasing overpressure) transitions to a reduction of subharmonic as the acoustic pressure exceeds the subharmonic threshold (a value in the range 200–300 kPa at 2 MHz excitation; Fig. 2b, 2c). Note that each data point is measured independently over different batches of microbubble solution, emphasizing the consistency of the observations. (See Experimental Procedure under Methods.)

For acoustic pressures in the growth-saturation stage (300–700 kPa), the decrease in subharmonic weakens as PNP increases; that is, the subharmonic exhibits the strongest sensitivity to overpressure at the beginning of this phase, consistent with the observation made by Shi et al. [21]. For low excitation amplitudes before occurrence (50–200 kPa), the change in subharmonic is positive though with a non-monotonic trend. The enhancement in subharmonic exhibits an apparent linear increase up to ~10 kPa overpressure (ascending part) followed by saturation and then diminishes for overpressures beyond 15 kPa (descending part). It seems that further increase in overpressure suppresses subharmonic generation, in agreement with the study of SonoVue by Nio et al. [31].

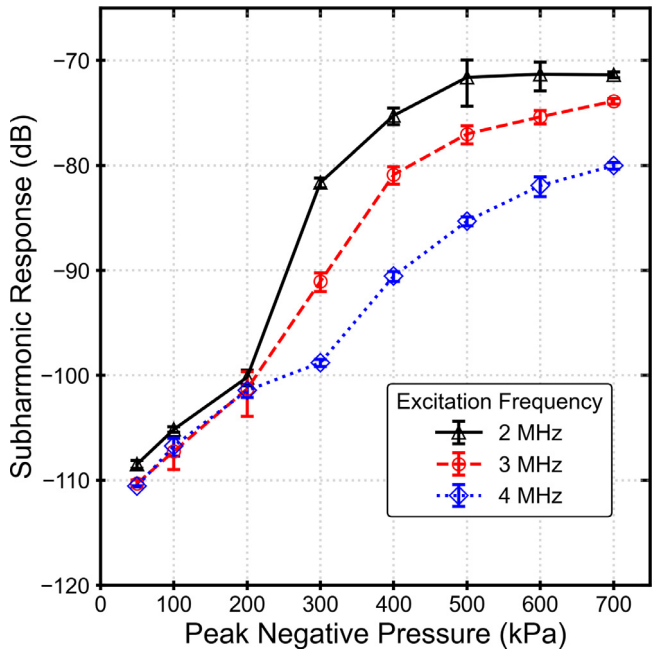

Figure 8. Subharmonic response as a function of peak negative pressure for different excitation frequencies.

Figure 4 depicts examples of the frequency domain responses of microbubbles, recording enhancement and reduction in subharmonic with overpressure. An overpressure of 15 kPa resulted in an average enhancement of 10.78 dB in subharmonic at 100 kPa peak negative pressure and 2 MHz frequency excitation (Fig. 4a). On the other hand, applying 25 kPa overpressure resulted in an average 13.78 dB reduction in subharmonic amplitude at 300 kPa acoustic peak negative pressure and 2 MHz frequency (Fig. 4b). Note the relatively small change in other harmonics (fundamental: 2 MHz, second harmonic: 4 MHZ, ultraharmonic: 3 MHz). The ambient pressure sensitivity of these harmonics is discussed later.

Figure 5 reveals a linear fit applied to the subharmonic changes with overpressure in both the decreasing and increasing regimes in Figure 3f. The correlation coefficients (R^2) larger than 0.9 indicate strong linearity, with the slope of the linear fit signaling the strength of sensitivity to overpressure. Figure 5a illustrates a sensitivity of −0.56 dB/kPa, which is comparable to previous studies on commercial contrast agents (Table 1). For the non-monotonic increasing trend, subharmonic sensitivity for ascending (0–10 kPa) and descending (15–25 kPa) parts are 1.08 and −0.71 dB/kPa, respectively.

Figure 6 illustrates subharmonic sensitivity to overpressure at higher excitation frequencies (3 and 4 MHz). In general, here the behaviors are like those at 2 MHz excitation; at lower excitation pressures, subharmonic increases with overpressure, and at higher excitations, subharmonic decreases under overpressure. At lower excitations (increasing regime), a non-monotonic trend similar to that for the 2 MHz excitation case is noted (Fig. 3f), with the increase reaching a maximum at 15 kPa overpressure. However, in the decreasing regime, the reduction in subharmonic is significantly smaller in comparison to 2 MHz excitation. In addition, the transition from an increasing to a decreasing trend occurs at different excitation amplitudes. At 4 MHz (Fig. 6b) for 300 kPa peak negative pressure excitation, subharmonic increases with overpressure in contrast to that at 2 MHz excitation, where for the same excitation strength a linear decrease was observed.

Figure 7 illustrates the corresponding frequency domain responses before and after ambient sensitivity trend transition for 3 and 4 MHz frequencies, revealing the growth of subharmonic amplitude after the transition points. Like the 2 MHz case, here also the transition point is closely related to the subharmonic threshold, which is in the ranges 200–300 and 300–400 kPa for 3 MHz (Fig. 7a) and 4 MHz (Fig. 7b), respectively. One can conclude that the increasing trend coincides with the range of excitations below the threshold (at atmospheric pressure), while the decreasing trend coincides with the growth-saturation stage for all frequencies considered here. Indeed, in Figure 8, plotting the subharmonic as a function of PNP, we note that the occurrence growth saturation curves shift toward higher PNPs for higher frequencies—the threshold for a particular level of the subharmonic signal (*e.g.,* −90 dB) shifts to higher PNP values at higher frequencies.

Effects of overpressure on the fundamental, second harmonic and ultraharmonic are illustrated in Figure 9. The fundamental response exhibits weak sensitivity to the overpressure with slightly decreasing trends for all excitations. The second harmonic in our experiment exhibited an atypical behavior, while for most acoustic excitations it changed little with ambient overpressure. At the lowest excitation of 50 kPa, it showed a significant increase of 8 dB at 2 MHz and a slightly increasing trend for 100 kPa at 3 and 4 MHz. The ultraharmonic (of 3/2 order) exhibited a noticeable decreasing trend with overpressure for acoustic excitations corresponding to the growth stage. Unlike for the subharmonic, overpressure does not trigger ultraharmonic generation below the threshold corresponding to atmospheric pressure. Finally, the subharmonic change with overpressure, which, unlike the other harmonics, exhibits the strongest sensitivity, is summarized in Table 3.

Discussion and conclusion

The results of the current study indicate that for all the frequencies considered, at lower excitations, when at atmospheric pressure there is no subharmonic; the subharmonic occurs and increases with overpressure, but at higher excitations (*i.e.,* corresponding to the growth-saturation phase at zero overpressure), it decreases with overpressure. In other words, the decreasing or increasing trend depends on threshold values at atmospheric pressure. The appearance of subharmonic response only under overpressure presents the possibility of a medical "go–no go" gauge, potentially offering quick, repeatable and easy-to-interpret preliminary examinations, provided that sufficient signals can be detected at the lower excitations [46].

This phenomenon may explain the previous experimental results as well. Xu et al. [30] observed an increase in the subharmonic from SonoVue microbubbles with overpressure, increasing from 10 to 40 mm Hg (~1–5 kPa) at low excitations (40–300 kPa) but decreasing at higher excitations (400–540 kPa). Similarly, Nio et al. [31] observed a linear increase in subharmonic from SonoVue with ambient pressure increased up to 75 mmHg (~10 kPa) at excitations up to 300 kPa. However, a further increase above 75 to 200 mmHg (~ 26 kPa) resulted in saturation followed by a decline in subharmonic enhancement by overpressure. Li et al. [47] observed the non-monotonic behavior of a subharmonic at 4 MHz and 350 kPa excitation for SonoVue; it first increased with overpressure up to 50 mmHg (~6 kPa) and then decreased. The non-monotonic trend, however, changed to a linear decrease at a lower frequency of 1.33 MHz. Note that we also noted behavior is dependent on the excitation frequency (Figs. 6 and 3f); in Figure 6, the change in subharmonic at a PNP of 300 kPa transforms from a non-monotonic trend at 4 MHz to a monotonic decrease at 3 MHz. The behavior stems primarily from the dependence of subharmonic threshold on frequency (Fig. 8). The subharmonic thresholds recorded in this study (200–400 kPa) are similar to those in previous studies on commercial phospholipid microbubbles with a size distribution similar to that of our in-house–made bubble [21,48–50]. For lipid microbubbles with a C_4F_{10} gas core (in contrast to SonoVue with a SF_6 gas core) and average radius of 2 μm, Frinking et al. [29] also observed an increase in subharmonic response at low acoustic excitations (<350 kPa; *i.e.,* at occurrence stage) with overpressure, but a decrease at higher excitations.

We have here related the transition from an increasing to a decreasing trend in subharmonic with overpressure increase to the subharmonic

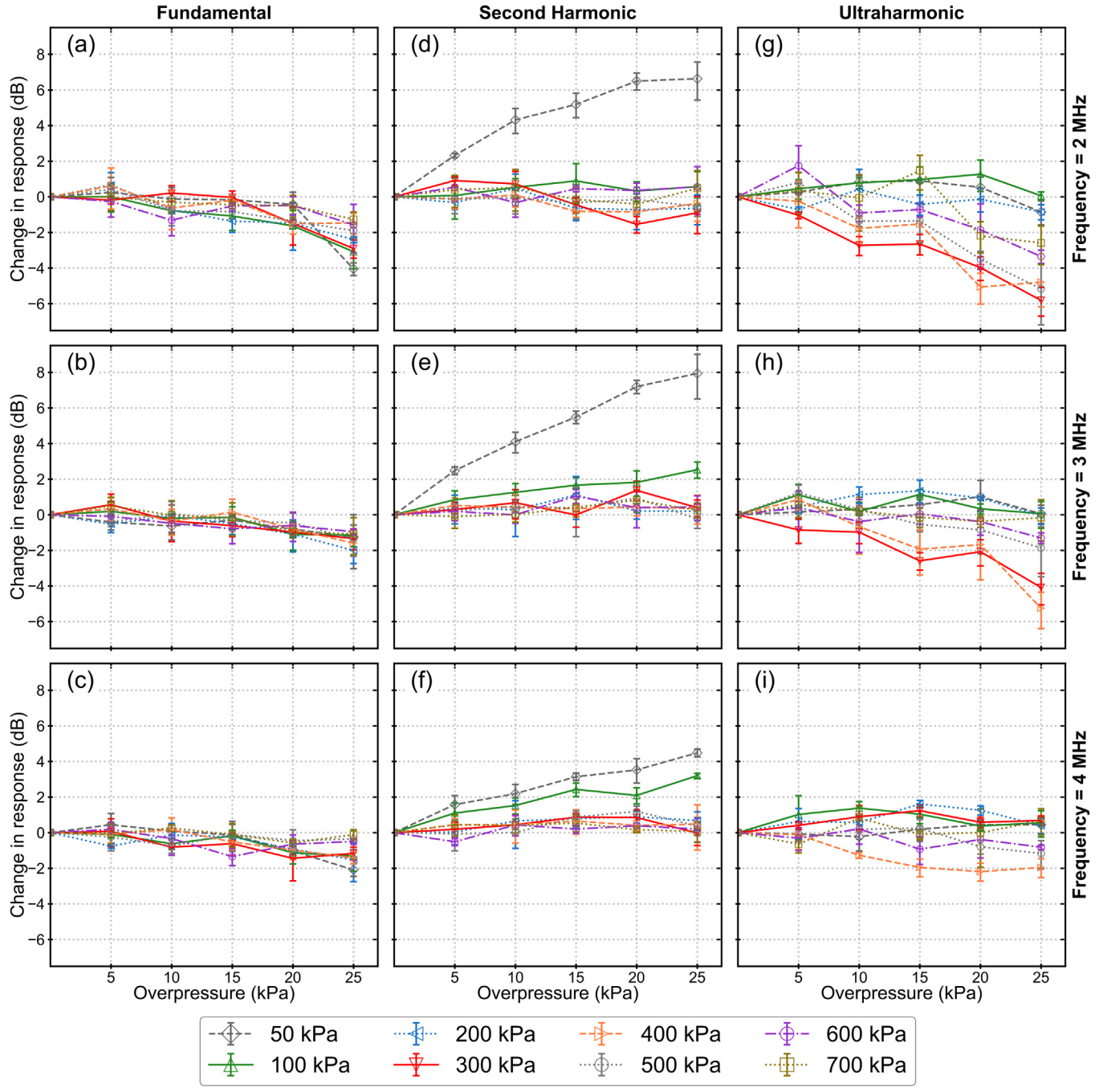

Figure 9. Ambient pressure sensitivity of fundamental (a–c), second harmonic (d–f) and ultraharmonic (g–i) at acoustic pressures of 50–700 kPa and excitation frequencies of 2–4 MHz.

Table 3
Subharmonic sensitivity measured in this study

Frequency (MHz)	Overpressure (kPa)	PNP (kPa)	Trend	Maximum change/ sensitivity
2	0–25	50–200	Increase	10.78 dB
		300–700	Decrease	0.56 dB/kPa
3	0–25	50–200	Increase	10.23 dB
		300–700	Decrease	0.3 dB/kPa
4	0–25	50–300	Increase	7.92 dB
		400–700	Decrease	0.24 dB/kPa

PNP, peak negative pressure.

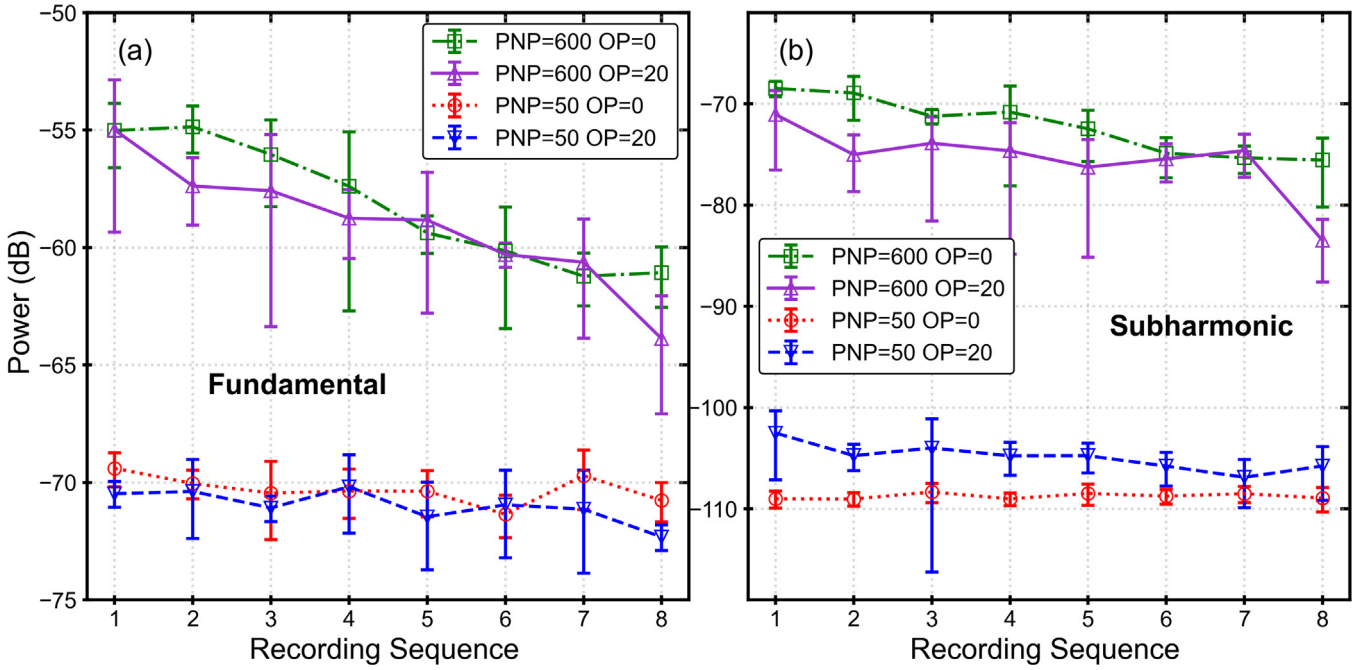

Figure 10. Acoustic response of microbubbles undergoing eight pressurizing cycles of 0 and 25 kPa overpressures (OP) at 600 and 50 kPa peak negative pressures (PNPs) as a function of recording sequence (*i.e.,* time). (a) Fundamental; (b) subharmonic.

threshold value at atmospheric pressure. Below the threshold excitation, increasing overpressure increases subharmonic response, whereas above the threshold, in the growth-saturation regime, increasing overpressure decreases subharmonic response. Furthermore, the increasing trend in the former region stems from the lowering of the threshold excitation by increased overpressure from its value at 1 atm. Note that the increasing trend has not been seen *in vivo*, possibly because of their occurrence only at lower excitations.

The subharmonic increase with overpressure at low excitations previously observed was attributed to the increase in compression-only behavior caused by buckling of the microbubble resulting from overpressure [29,51], which has been reported to be associated with subharmonic generation [52,53]. Frinking et al. used the Marmottant model [34] to illustrate compression-only behavior and the presence of subharmonic in a buckled state (zero surface tension) but not in an elastic state (surface tension = 0.02 N/m). Note that the buckling is attributed to change in size caused by overpressure, which for zero gas exchange is limited to less than 10% [35]. Size change also affects the resonance frequency of a bubble with significant impact on the subharmonic response as we noted before [40]. Incidentally, Tremblay-Darveau et al. [18] reported that the resonance frequency change in lipid-coated microbubbles in the transition regime between the elastic and the buckled states can be used in blood pressure measurement. The eventual decrease in subharmonic at higher overpressures possibly indicates a severe restriction of bubble activities. Nio et al. [31] concluded that this is due to the destruction of microbubbles under elevated hydrostatic pressures. However, we found that the fundamental and subharmonic responses returned to their baseline values when the overpressure was released at low PNP (Fig. 10), indicating that microbubble destruction caused by overpressure is minimal at this low excitation. At a higher PNP of 600 kPa, we do see decay of the acoustic response over eight pressurizing cycles, indicating some destruction caused by high acoustic pressures. However, the change in response remains approximately constant over eight cycles (Fig. 10). Frinking et al. [29,54] attributed the reduction in subharmonic with overpressure in the decreasing regime to the decrease in the size of free microbubbles generated by the destruction of the shell. However, the fundamental response exhibited almost constant sensitivity for all peak negative pressures and frequencies (Fig. 9a–c), implying that microbubble destruction does not significantly affect the sensitivity.

The enhancement value of the subharmonic for low excitations (in the increasing regime) remains similar for different frequencies. However, for higher excitations (in the decreasing regime), the sensitivity varies for different frequencies (Table 3). The atypical behavior of the second harmonic at 50 kPa acoustic pressure demands further investigation. Note that using Marmottant model, Tremblay-Darveau et al. [18] found that in the transition between elastic and buckled states, a strong second harmonic exists even at a low acoustic pressure (1–10 kPa). The similar threshold of sub- and ultraharmonic generation and their behavior in the regime of decreasing trends point to their similar non-linear nature. However, the lack of overpressure-driven ultraharmonic generation contrasts with the subharmonic, and thereby only a decreasing trend with overpressure is observed in the ultraharmonic frequency component.

The higher ambient pressure sensitivity of subharmonic compared with other harmonics points to its suitability for pressure estimation in medical applications. In addition to the linear decrease in subharmonic with ambient pressure at higher excitations currently used for SHAPE, the linearly increasing section at lower pressure can potentially be used in applications dealing with lower blood pressures (<10 kPa), where higher sensitivity (see Fig. 5: 1.08 dB/kPa vs. 0.56 dB/kPa) is needed if a sufficient signal can be detected.

Conflict of interest

The authors declare no competing interests.

Acknowledgments

R.H.A. acknowledges helpful discussions with Dr. Kourosh Kalayeh and assistance from Nicholas Batista and Emanuel Mafilios for the experimental setup. K.S., F.F. and J.R.E. acknowledge partial support from National Institutes of Health Award R01EB032333. K.S. acknowledges partial support from National Science Foundation Award 2037849.

Data availability statement

The data sets generated and/or analyzed during the current study are available from the corresponding author on reasonable request.

References

[1] De Jong N. Current and new methods of ultrasound. Anaesthesist 2015;64:874–83.
[2] Kooiman K, Vos HJ, Versluis M, de Jong N. Acoustic behavior of microbubbles and implications for drug delivery. Adv Drug Deliv Rev 2014;72:28–48.
[3] de Jong N, Bouakaz A, Frinking P. Basic acoustic properties of microbubbles. Echocardiography 2002;19:229–40.
[4] de Jong N, Emmer M, van Wamel A, Versluis M. Ultrasonic characterization of ultrasound contrast agents. Med Biol Eng Comput 2009;47:861–73.
[5] Shankar PM, Krishna PD, Newhouse VL. Advantages of subharmonic over second harmonic backscatter for contrast-to-tissue echo enhancement. Ultrasound Med Biol 1998;24:395–9.
[6] Shi WT, Forsberg F, Hall AL, Chiao RY, Liu JB, Miller S, et al. Subharmonic imaging with microbubble contrast agents: initial results. Ultrason Imaging 1999;21:79–94.
[7] Forsberg F, Shi WT, Goldberg BB. Subharmonic imaging of contrast agents. Ultrasonics 2000;38:93–8.
[8] Forsberg F, Piccoli CW, Sridharan A, Wilkes A, Sevrukov A, Ojeda-Fournier H, et al. 3D harmonic and subharmonic imaging for characterizing breast lesions: a multicenter clinical trial. J Ultrasound Med 2022;41:1667–75.
[9] Eisenbrey JR, Sridharan A, Machado P, Zhao H, Halldorsdottir VG, Dave JK, et al. Three-dimensional subharmonic ultrasound imaging in vitro and in vivo. Acad Radiol 2012;19:732–9.
[10] Goertz DE, Cherin E, Needles A, Karshafian R, Brown AS, Burns PN, et al. High frequency nonlinear B-scan imaging of microbubble contrast agents. IEEE Trans Ultrason Ferroelectr Freq Control 2005;52:65–79.
[11] Goertz DE, Frijlink ME, Tempel D, Bhagwandas V, Gisolf A, Krams R, et al. Subharmonic contrast intravascular ultrasound for vasa vasorum imaging. Ultrasound Med Biol 2007;33:1859–72.
[12] Needles A, Arditi M, Rognin NG, Mehi J, Coulthard T, Bilan-Tracey C, et al. Nonlinear contrast imaging with an array-based micro-ultrasound system. Ultrasound Med Biol 2010;36:2097–106.
[13] Dave JK, Halldorsdottir VG, Eisenbrey JR, Raichlen JS, Liu JB, McDonald ME, et al. Subharmonic microbubble emissions for noninvasively tracking right ventricular pressures. Am J Physiol Heart Circ Physiol 2012;303:H126–32.
[14] Dave JK, Halldorsdottir VG, Eisenbrey JR, Forsberg F. Processing of subharmonic signals from ultrasound contrast agents to determine ambient pressures. Ultrason Imaging 2012;34:81–92.
[15] Dave JK, Halldorsdottir VG, Eisenbrey JR, Merton DA, Liu JB, Machado P, et al. On the implementation of an automated acoustic output optimization algorithm for subharmonic aided pressure estimation. Ultrasonics 2013;53:880–8.
[16] Shankar PM, Chapelon JY, Newhouse VL. Fluid pressure measurement using bubbles insonified by two frequencies. Ultrasonics 1986;24:333–6.
[17] Fairbank Jr. WM, Scully MO. A new noninvasive technique for cardiac pressure measurement: resonant scattering of ultrasound from bubbles. IEEE Trans Biomed Eng 1977;24:107–10.
[18] Tremblay-Darveau C, Williams R, Burns PN. Measuring absolute blood pressure using microbubbles. Ultrasound Med Biol 2014;40:775–87.
[19] Hok B. A new approach to noninvasive manometry: interaction between ultrasound and bubbles. Med Biol Eng Comput 1981;19:35–9.
[20] Bouakaz A, Frinking PJA, de Jong N, Bom N. Noninvasive measurement of the hydrostatic pressure in a fluid-filled cavity based on the disappearance time of micrometer-sized free gas bubbles. Ultrasound Med Biol 1999;25:1407–15.
[21] Shi W, Forsberg F, Raichlen J, Needleman L, Goldberg B. Pressure dependence of subharmonic signals from contrast microbubbles. Ultrasound Med Biol 1999;25:275–83.
[22] Dave JK, Halldorsdottir VG, Eisenbrey JR, Raichlen JS, Liu JB, McDonald ME, et al. Noninvasive LV pressure estimation using subharmonic emissions from microbubbles. JACC Cardiovasc Imaging 2012;5:87–92.
[23] Halldorsdottir VG, Dave JK, Eisenbrey JR, Machado P, Zhao H, Liu JB, et al. Subharmonic aided pressure estimation for monitoring interstitial fluid pressure in tumours —in vitro and in vivo proof of concept. Ultrasonics 2014;54:1938–44.
[24] Halldorsdottir VG, Dave JK, Marshall A, Forsberg AI, Fox TB, Eisenbrey JR, et al. Subharmonic-aided pressure estimation for monitoring interstitial fluid pressure in tumors: calibration and treatment with paclitaxel in breast cancer xenografts. Ultrasound Med Biol 2017;43:1401–10.
[25] Gupta I, Eisenbrey JR, Machado P, Stanczak M, Wessner CE, Shaw CM, et al. Diagnosing portal hypertension with noninvasive subharmonic pressure estimates from a US contrast agent. Radiology 2021;298:104–11.
[26] Eisenbrey JR, Dave JK, Halldorsdottir VG, Merton DA, Miller C, Gonzalez JM, et al. Chronic liver disease: noninvasive subharmonic aided pressure estimation of hepatic venous pressure gradient. Radiology 2013;268:581–8.
[27] Dave JK, Halldorsdottir VG, Eisenbrey JR, Merton DA, Liu JB, Zhou JH, et al. Investigating the efficacy of subharmonic aided pressure estimation for portal vein pressures and portal hypertension monitoring. Ultrasound Med Biol 2012;38:1784–98.
[28] Prosperetti A. Subharmonics and ultraharmonics in the forced oscillations of weakly nonlinear systems. Am J Phys 1976;44:548–54.
[29] Frinking PJ, Brochot J, Arditi M. Subharmonic scattering of phospholipid-shell microbubbles at low acoustic pressure amplitudes. IEEE Trans Ultrason Ferroelectr Freq Control 2010;57:1762–71.
[30] Xu G, Lu H, Yang H, Li D, Liu R, Su M, et al. Subharmonic scattering of sonovue microbubbles within 10−40-mmHg overpressures in vitro. IEEE Trans Ultrason Ferroelectr Freq Control 2021;68:3583–91.
[31] Nio AQX, Faraci A, Christensen-Jeffries K, Raymond JL, Monaghan MJ, Fuster D, et al. Optimal control of SonoVue microbubbles to estimate hydrostatic pressure. IEEE Trans Ultrason Ferroelectr Freq Control 2020;67:557–67.
[32] Gupta I, Nio AQX, Faraci A, Torkzaban M, Christensen-Jeffries K, Nam K, et al. The effects of hydrostatic pressure on the subharmonic response of sonovue and Sonazoid. Proc IEEE Int Ultrasound Symp 2019:1349–52.
[33] Faez T, Renaud G, Defontaine M, Calle S, de Jong N. Dynamic manipulation of the subharmonic scattering of phospholipid-coated microbubbles. Phys Med Biol 2011;56:6459–73.
[34] Marmottant P, van der Meer S, Emmer M, Versluis M, de Jong N, Hilgenfeldt S, et al. A model for large amplitude oscillations of coated bubbles accounting for buckling and rupture. J Acoust Soc Am 2005;118:3499–505.
[35] Kumar KN, Sarkar K. Interfacial rheological properties of contrast microbubble Targestar P as a function of ambient pressure. Ultrasound Med Biol 2016;42:1010–7.
[36] Kumar KN, Sarkar K. Effects of ambient hydrostatic pressure on the material properties of the encapsulation of an ultrasound contrast microbubble. J Acoust Soc Am 2015;138:624–34.
[37] Segers T, Gaud E, Versluis M, Frinking P. High-precision acoustic measurements of the nonlinear dilatational elasticity of phospholipid coated monodisperse microbubbles. Soft Matter 2018;14:9550–61.
[38] Katiyar A, Sarkar K. Excitation threshold for subharmonic generation from contrast microbubbles. J Acoust Soc Am 2011;130:3137–47.
[39] Katiyar A, Sarkar K. Effects of encapsulation damping on the excitation threshold for subharmonic generation from contrast microbubbles. J Acoust Soc Am 2012;132:3576–85.
[40] Katiyar A, Sarkar K, Forsberg F. Modeling subharmonic response from contrast microbubbles as a function of ambient static pressure. J Acoust Soc Am 2011;129:2325–35.
[41] Azami RH, Aliabouzar M, Osborn J, Kumar KN, Forsberg F, Eisenbrey JR, et al. Material properties, dissolution and time evolution of PEGylated lipid-shelled microbubbles: effects of the polyethylene glycol hydrophilic chain configurations. Ultrasound Med Biol 2022;48:1720–32.
[42] Aliabouzar M, Kumar KN, Sarkar K. Effects of droplet size and perfluorocarbon boiling point on the frequency dependence of acoustic vaporization threshold. J Acoust Soc Am 2019;145:1105.
[43] Brewin MP, Pike LC, Rowland DE, Birch MJ. The acoustic properties, centered on 20 MHz, of an IEC agar-based tissue-mimicking material and its temperature, frequency and age dependence. Ultrasound Med Biol 2008;34:1292–306.
[44] Mikeska EE, Behrens JA. Evaluation of transducer window materials. J Acoust Soc Am 1976;59:1294–8.
[45] Lee JH, Kim BN, Shin KK, Yoon SW. Insertion loss of sound waves through composite acoustic window materials. Curr Appl Phys 2010;10:138–44.
[46] Machado P, Gupta I, Gummadi S, Stanczak M, Wessner CE, Fenkel JM, et al. Hepatic vein contrast-enhanced ultrasound subharmonic imaging signal as a screening test for portal hypertension. Dig Dis Sci 2021;66:4354–60.
[47] Li F, Li D, Yan F. Improvement of detection sensitivity of microbubbles as sensors to detect ambient pressure. Sensors (Basel) 2018;18:4083.
[48] Shekhar H, Awuor I, Thomas K, Rychak JJ, Doyley MM. The delayed onset of subharmonic and ultraharmonic emissions from a phospholipid-shelled microbubble contrast agent. Ultrasound Med Biol 2014;40:727–38.
[49] Sarkar K, Shi WT, Chatterjee D, Forsberg F. Characterization of ultrasound contrast microbubbles using in vitro experiments and viscous and viscoelastic interface models for encapsulation. J Acoust Soc Am 2005;118:539–50.
[50] Helfield BL, Cherin E, Foster FS, Goertz DE. Investigating the subharmonic response of individual phospholipid encapsulated microbubbles at high frequencies: a comparative study of five agents. Ultrasound Med Biol 2012;38:846–63.
[51] Qiao X, Wen Y, Yu J, Bouakaz A, Zong Y, Wan M. Noninvasive pressure estimation based on the subharmonic response of SonoVue: application to intracranial blood pressure assessment. IEEE Trans Ultrason Ferroelectr Freq Control 2022;69:957–66.
[52] Sijl J, Dollet B, Overvelde M, Garbin V, Rozendal T, de Jong N, et al. Subharmonic behavior of phospholipid-coated ultrasound contrast agent microbubbles. J Acoust Soc Am 2010;128:3239–52.
[53] de Jong N, Emmer M, Chin CT, Bouakaz A, Mastik F, Lohse D, et al. Compression-only" behavior of phospholipid-coated contrast bubbles. Ultrasound Med Biol 2007;33:653–6.
[54] Chomas J, Dayton P, May D, Ferrara K. Nondestructive subharmonic imaging. IEEE Trans Ultrason Ferroelectr Freq Control 2002;49:883–92.
[55] Kalayeh K, Fowlkes JB, Chen A, Yeras S, Fabiilli ML, Claflin J, et al. Pressure measurement in a bladder phantom using contrast-enhanced ultrasonography—a path to a catheter-free voiding cystometrogram. Invest Radiol 2023;58:181–9.
[56] Sun T, Jia N, Zhang D, Xu D. Ambient pressure dependence of the ultra-harmonic response from contrast microbubbles. J Acoust Soc Am 2012;131:4358–64.
[57] Halldorsdottir VG, Dave JK, Leodore LM, Eisenbrey JR, Park S, Hall AL, et al. Subharmonic contrast microbubble signals for noninvasive pressure estimation under static and dynamic flow conditions. Ultrason Imaging 2011;33:153–64.
[58] Andersen KS, Jensen JA. Impact of acoustic pressure on ambient pressure estimation using ultrasound contrast agent. Ultrasonics 2010;50:294–9.
[59] Adam D, Sapunar M, Burla E. On the relationship between encapsulated ultrasound contrast agent and pressure. Ultrasound Med Biol 2005;31:673–86.
[60] Dave JK, Halldorsdottir VG, Eisenbrey JR, Liu JB, McDonald ME, Dickie K, et al. Noninvasive estimation of dynamic pressures in vitro and in vivo using the subharmonic response from microbubbles. IEEE Trans Ultrason Ferroelectr Freq Control 2011;58:2056–66.